CU Journal of Non-Linear Fluid Mechanics
Vol. 01, No. 02, 2025
https://doi.org/10.11615/cujnlfm.01204-0

Study of Pre-Chaotic and Post-Chaotic Motions in Internal Heat Generation Driven Convection of Palm Oil-Based Nanoliquids: Rigid-Rigid Boundaries

P. G. Siddheshwar *[a]

[a] Centre for Mathematical Needs, Department of Mathematics, Christ University, Bengaluru 560029, India

Abstract

The paper investigates both linear and non-linear regimes of convection in nanoliquids having palm-oil as the base with internal-heat-generation ($\mathscr{IHG}$) dominating buoyancy. Palm oil is used with well-dispersed nanoparticles of either copper or titanium dioxide. We adopt a formulation that gives an $\mathscr{IHG}$- based Rayleigh number as an eigenvalue. The effective thermophysical properties are evaluated using mixture theory and phenomenological models, leading to a modified Rayleigh number that involves a dimensionless factor, F, representing the influence of nanoparticles loading. The Maclaurin series expansion method is used in the linear stability analysis to represent the eigen function as a power series. For the nonlinear regime, the Galerkin-Fourier method helped in deriving the generalized-Lorenz-model and thereby the Stuart–Landau equation is arrived at to describe the amplitude evolution near the convection threshold. The approach enhances understanding of how internal heat generation affects convective and chaotic flows in nanoliquids and offers valuable guidance for optimizing thermal management and energy system performance. Palm oil-based nanoliquids containing either copper or titanium dioxide nanoparticles have contrasting thermal and chemical properties and lead to distinct enhancements in heat transfer performance, stability, and response to $\mathscr{IHG}$. Chaotic motion is shown to be impossible in the considered palm-oil-based nanoliquids due to them being high Prandtl number liquids. The results of the problem have immense applications in thermal energy problems involving coolants and also in thermal-storage devices.

Keywords: Internal heat generation; Convection; Semi-analytical method; Linear stability; Nonlinear stability; Boundary eigenvalue problem.

1 Introduction

The study of internally heated convection has long been a central theme in fluid mechanics due to its broad relevance to geophysical, astrophysical, and industrial systems. The inital experimental work of Tritton and Zarraga [1] revealed that when a fluid layer of infinite horizontal extent is subjected to $\mathscr{IHG}$, cellular convection structures develop in a manner similar to classical Bénard type convection. Their observations also showed the practical significance of such flows, including their possible connection to convection processes within the Earth's mantle. Subsequently based on these findings, Roberts [2] presented a theoretical framework for convection in a uniformly

* pg.siddheshwar@christuniversity.in

heated layer and derived the corresponding critical-Rayleigh-number and wave-number at the onset-of-convection. Using a numerical method, Thirlby [3] later confirmed these results and demonstrated how the Rayleigh and Prandtl numbers affect the flow morphology. Schwiderski [4], Peckover and Hutchinson [5], and Gasser and Kazimi [6] further extended the above theoretical studies by studying the stability behavior, influence of boundaries and the impact of $\mathscr{IHG}$.

The classical Bénard problem has been studied with modifications introduced through the inclusion of additional physical effects. The work of Hamabata and Takashima [7] studied the influence of rotation, while Tasaka and Takeda [8], and Kuznetsov and Nield [9] investigated non-uniform $\mathscr{IHG}$. Their analysis highlighted that internal heating interacts strongly with mechanisms such as rotation, which can postpone the onset of convection depending on system parameters. Modern high Rayleigh number simulations by Goluskin and van der Poel [10], and Wang et al.[11] have provided scaling relationships that connect mean temperature, convective stability, and heat transport. Deepika et al.[12] extended such a study by considering convection in a Darcy–Brinkman-porous-medium along with effects of throughflow and $\mathscr{IHG}$.

In recent years, interest has increasingly shifted from conventional fluids to nanofluids, which are fluids that contain nanosized particles uniformly dispersed within a base liquid to enhance thermal performance. Efficient cooling plays an important role in a wide range of mechanical and electronic applications. Earlier attempts to improve thermal behavior through the addition of micron-sized solid particles yielded some benefits but also introduced challenges such as sedimentation and clogging. Use of nanoparticles, with their much smaller size and higher surface area, addressed the drawbacks by offering improved suspension stability and superior heat transfer capability. When nanoparticles are dispersed in a base fluid, they modify its key thermophysical properties such as viscosity, density, and thermal conductivity which in turn influence its convective behavior and overall heat transfer performance.

Choi [13] introduced nanoliquids which was obtained by dispersing nanoscale particles in a base liquid to enhance heat transfer. Eastman et al.[14] experimentally observed a notable rise in the thermal-conductivity of ethylene-glycol-based nanoliquids, igniting substantial research interest. Later, Das et al.[15] demonstrated the strong temperature-dependence of this enhancement, and Buongiorno [16] formulated a two-phase transport model incorporating Brownian diffusion and thermophoresis as principal nanoparticle mechanisms. These works helped the practical use of nanofluids in engineering, giving us the mechanism for their adoption in areas such as solar energy harvesting, cooling of microelectronic devices, and other thermal management applications.

The modelling of Rayleigh–Bénard-Convection ($\mathscr{RBC}$) in nanoliquids is carried out using the Khanafer–Vafai–Lightstone ($\mathscr{KVL}$) single-phase model [17] or the Buongiorno two-phase model [16]. Siddheshwar et al. ([18], [19]) generalised the Buongiorno model [16] to include thermophysical properties of the base liquid and nanoparticles and verified the thermdynamic validity of both formulations and demonstrated their ability to describe heat transfer enhancement in nanoliquid convection. Kanchana and Laroze[20] used a generalized-Lorenz-model to analyze water–alumina nanoliquids containing internal heat sources and sinks. Their analysis revealed that nanoparticles' addition has a stabilizing effect on the convective process, even when considering chaotic motion.

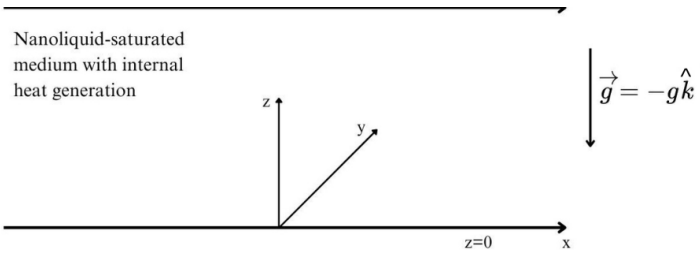

Figure 1: Physical configuration of the problem.

The current study extends this body of work by exploring $\mathscr{IHG}$ in nanoliquids having palm-oil as the base and with either copper (Cu) or titanium dioxide (TiO_2) nanoparticles. Palm oil has gained attention as a sustainable base fluid because of its suitable viscosity and good thermal stability. When dispersed with Cu or TiO_2 nanoparticles, the overall thermal conductivity of palm oil increases significantly, making it a promising option as an environmentally friendly nanoliquid for heat transfer applications. The mathematical framework employs the Maclaurin series-based eigenvalue estimation technique discussed in the works of [21], [22], [23], [24]. The study on $\mathscr{IHG}$ convection remains largely unexplored, particularly for palm oil-based Cu/TiO_2 nanoliquids for the case of rigid–rigid boundary condition. This investigation aims to fill that gap and provide new insights into the stability characteristics of thermally driven nanofluid systems.

2 Mathematical Formulation

We consider a fluid layer of infinite horizontal extent and of thickness d, whose lower and upper bounding planes are at $z = 0$ and $z = d$, respectively. The lower-boundary is rigid-adiabatic, while the upper-one is free-isothermal. The fluid-density is ρ_{nl}, the dynamic viscosity is μ_{nl}, the thermal-diffusivity is χ_{nl}, fluid-velocity is $\vec{q} = (u, 0, w)$ and the coefficient-of-thermal-expansion is β_{nl}. The subscript nl denotes nanoliquid and np denotes nanoparticle. The internal-heating is evenly distributed throughout the fluid layer, resulting in an $\mathscr{IHG}$ term, Q, in the equation of conservation-of-energy.

In formulating the governing-equations, we have made use of the Boussinesq-approximation as a result of which density remains constant except where it is multiplied by gravity. The governing-equations are as follows:

Conservation-of-Mass:

$$\nabla \cdot \vec{q} = 0, \tag{1}$$

Conservation-of-Linear- Momentum:

$$\rho_{nl}\left[\frac{\partial \vec{q}}{\partial t} + (\vec{q}\cdot\nabla)\vec{q}\right] = -\nabla p + \mu_{nl}\nabla^2\vec{q} - \rho_{nl}\left[1 - \beta_{nl}(T - T_0)\right] g\mathbf{k}, \tag{2}$$

Conservation-of-Energy:

$$\left(\frac{\partial}{\partial t}+(\vec{q}\cdot\nabla)-\chi_{nl}\nabla^2\right)T=Q, \tag{3}$$

Phenomenological-Laws:

$$\left.\begin{aligned}\frac{\mu_{nl}}{\mu_{bl}}&=\frac{1}{(1-\alpha)^{2.5}},\\ \frac{k_{nl}}{k_{bl}}&=\frac{\left(\frac{k_{np}}{k_{bl}}+2\right)-2\alpha\left(1-\frac{k_{np}}{k_{bl}}\right)}{\left(\frac{k_{np}}{k_{bl}}+2\right)+\alpha\left(1-\frac{k_{np}}{k_{bl}}\right)}\end{aligned}\right\}, \tag{4}$$

Mixture theory:

$$\left.\begin{aligned}\chi_{bl}=\frac{k_{bl}}{(\rho C_p)_{bl}},\ \chi_{nl}&=\frac{k_{nl}}{(\rho C_p)_{nl}},\\ \frac{\rho_{nl}}{\rho_{bl}}&=(1-\alpha)+\alpha\frac{\rho_{np}}{\rho_{bl}},\\ (\rho C_p)_{nl}&=(1-\alpha)+\alpha\frac{(\rho C_p)_{np}}{(\rho C_p)_{bl}},\\ (\rho\beta)_{nl}&=(1-\alpha)+\alpha\frac{(\rho\beta)_{np}}{(\rho\beta)_{bl}}\end{aligned}\right\}. \tag{5}$$

Considering Eqs. (1), (2) and (3) in component-form, we get

$$\begin{bmatrix}\frac{\partial}{\partial x} & \frac{\partial}{\partial y}\end{bmatrix}\begin{bmatrix}u\\ v\end{bmatrix}=0, \tag{6}$$

$$\begin{bmatrix}\rho_{nl}\left(\frac{\partial}{\partial t}+u\frac{\partial}{\partial x}+w\frac{\partial}{\partial z}\right)-\mu_{nl}\nabla^2 & 0 & 0\\ 0 & \rho_{nl}\left(\frac{\partial}{\partial t}+u\frac{\partial}{\partial x}+w\frac{\partial}{\partial z}\right)-\mu_{nl}\nabla^2 & -\rho_{nl}\beta_{nl}\\ 0 & 0 & \frac{\partial}{\partial t}+u\frac{\partial}{\partial x}+w\frac{\partial}{\partial z}-\chi_{nl}\nabla^2\end{bmatrix}\begin{bmatrix}u\\ w\\ T\end{bmatrix}$$

$$=\begin{bmatrix}-\frac{\partial p}{\partial x}\\ -\frac{\partial p}{\partial z}-\rho_{nl}(1+\beta_{nl}T_0)\\ Q\end{bmatrix} \tag{7}$$

Using Eq. (6) and eliminating p between the first two equations of Eq. (7), we get the resulting-equation as:

$$\left[\rho_{nl}\left(\frac{\partial}{\partial t}+u\frac{\partial}{\partial x}+w\frac{\partial}{\partial z}\right)-\mu_{nl}\nabla^2 \quad (\rho\beta)_{nl}g\frac{\partial}{\partial x}\right]\begin{bmatrix}\zeta\\ T\end{bmatrix}=0, \tag{8}$$

where $\zeta = \begin{bmatrix} \frac{\partial}{\partial z} & -\frac{\partial}{\partial x} \end{bmatrix} \begin{bmatrix} u \\ w \end{bmatrix}$. The motion-less basic-state is governed by:

$$\left.\begin{aligned} (u_b, w_b) &= (0,0), \\ T_b(z) &= \frac{1-z^2}{2} \end{aligned}\right\}. \tag{9}$$

To make a stability analysis, we superimpose perturbations on the basic-state as:

$$(u,w) = (u_b + u', w_b + w'), \quad T = T_b(z) + T', \tag{10}$$

where prime indicates perturbed quantity. We reduce the number of dependent variables further on by introducing the stream function, ψ, as:

$$u' = -\frac{\partial \psi'}{\partial z} \text{ and } w' = \frac{\partial \psi'}{\partial x}. \tag{11}$$

Eq.(1) is satisfied in perturbed state also. We now adopt the following scaling which helps us in studying $\mathscr{I}\mathscr{H}\mathscr{G}$ convection:

$$(X,Z) = \left(\frac{x}{d}, \frac{z}{d}\right), \ \tau = \frac{t}{d^2/\chi_{bl}}, \Psi = \frac{\psi'}{\chi_{bl}}, \ \Theta = \frac{T'}{Qd^2/\chi_{bl}}, \tag{12}$$

we obtain the dimensionless form of the Eqs.(7) and (8) in terms of the stream function are:

$$\begin{bmatrix} \frac{1}{Pr_{nl}}\left(\frac{\partial}{\partial \tau} + \frac{\partial \Psi}{\partial X}\frac{\partial}{\partial Z} - \frac{\partial \Psi}{\partial Z}\frac{\partial}{\partial X}\right)\nabla^2 - a_1\nabla^4 & -Ra_{nl}a_1^3\frac{\partial}{\partial X} \\ -Z\frac{\partial}{\partial X} & \frac{\partial}{\partial \tau} + \frac{1}{Pr_{nl}}\left(\frac{\partial \Psi}{\partial X}\frac{\partial}{\partial Z} - \frac{\partial \Psi}{\partial Z}\frac{\partial}{\partial X}\right) - a_1\nabla^2 \end{bmatrix} \begin{bmatrix} \Psi \\ \Theta \end{bmatrix} = \begin{bmatrix} 0 \\ 0 \end{bmatrix} \tag{13}$$

where

$$Pr_{nl} = \frac{\mu_{nl}}{\rho_{nl}\chi_{bl}} \text{ is the nanoliquid Prandtl number,}$$

$$Ra = \frac{(\rho\beta)_{nl} g Q d^5}{(\mu\chi^2)_{nl}} \text{ is the nanoliquid Rayleigh number,}$$

and X is the non-dimensional horizontal coordinate, Z is the non-dimensional vertical coordinate, τ is the non-dimensional time, Ψ is the non-dimensional stream function, Θ is non-dimensional temperature, $a_1 = \frac{\chi_{nl}}{\chi_{bl}}$ and ∇^2 is the non- dimensional Laplacian. Eq. (13) is solved subject to

$$\begin{bmatrix} \frac{\partial}{\partial X} & 0 & 0 \\ \frac{\partial^2}{\partial X \partial Z} & 0 & 0 \\ 0 & 0 & \frac{\partial}{\partial Z} \end{bmatrix} \begin{bmatrix} \Psi \\ \Psi \\ \Theta \end{bmatrix}_{z=0} = \begin{bmatrix} 0 \\ 0 \\ 0 \end{bmatrix}, \tag{14}$$

$$\begin{bmatrix} \frac{\partial}{\partial X} & 0 & 0 \\ \frac{\partial^2}{\partial X \partial Z} & 0 & 0 \\ 0 & 0 & 1 \end{bmatrix} \begin{bmatrix} \Psi \\ \Psi \\ \Theta \end{bmatrix}_{z=1} = \begin{bmatrix} 0 \\ 0 \\ 0 \end{bmatrix}. \tag{15}$$

Eqs. (14) and (15) pertain to rigid-adiabatic and rigid-isothermal boundaries respectively. In the next section, we make a linear-stability-analysis to study the onset of pre-chaotic motion.

2.1 Linear Stability Analysis

We consider the normal mode solution:

$$\begin{bmatrix} \Psi \\ \Theta \end{bmatrix} = \begin{bmatrix} sin(aX)\ F(Z) \\ cos(aX)\ G(Z) \end{bmatrix}, \tag{16}$$

where $F(Z)$ and $G(Z)$ are amplitudes of the perturbations of the Ψ and Θ and a is the wave-number. Substituting Eq. (16) in Eq. (13), we arrive at the following equations:

$$\begin{bmatrix} a_1(D^2-a^2)^2 & -a_1^3 a^2 Ra_{nl} \\ Z & a_1(D^2-a^2) \end{bmatrix} \begin{bmatrix} F \\ G \end{bmatrix} = \begin{bmatrix} 0 \\ 0 \end{bmatrix} \tag{17}$$

where $D = \frac{d}{dZ}$. The boundary-condition to solve Eq. (17) can be got by substituting Eq. (16) in Eqs. (14)-(15) to get:

$$\begin{bmatrix} 1 & 0 & 0 \\ 0 & D & 0 \\ 0 & 0 & D \end{bmatrix} \begin{bmatrix} F \\ F \\ G \end{bmatrix}_{z=0} = \begin{bmatrix} 0 \\ 0 \\ 0 \end{bmatrix} \tag{18a}$$

$$\begin{bmatrix} 1 & 0 & 0 \\ 0 & D & 0 \\ 0 & 0 & 1 \end{bmatrix} \begin{bmatrix} F \\ F \\ G \end{bmatrix}_{z=1} = \begin{bmatrix} 0 \\ 0 \\ 0 \end{bmatrix} \tag{18b}$$

The critical-value of the eigenvalue, Ra_{nl}, and the wave-number, a, was reported by Roberts[2] who found them to be $Ra_{nl_c} = 2772.28$ and $a_c = 2.62$. The quantities Ra_{nl_c} and a_c obtained here are the same as that obtained by Roberts [2]. We use these values for Ra_{nl} and a in our subsequent calculations. Thus, having got Ra_{nl_c} and a_c, we will have to deal with an initial value problem now to obtain the normal modes as a power series. This procedure is explained further on.

2.2 Maclaurin series (MS) based solution: Semi-analytical approach

To solve Eq. (17) with the Eqs. (18a)-(18b), we need to convert the boundary-value-problem ($\mathscr{BVP}$) with a known eigen-value to an initial-value-problem ($\mathscr{IVP}$), with Ra_{nl} and a replaced by 2272.28 and 2.62 respectively. Next, we replace the right-end boundary-condition ($\mathscr{REBC}$) in Eq. (18b) with the unknown initial conditions:

$$\frac{\mathrm{d}^2\mathrm{F}}{\mathrm{d}Z^2}(0) = \tilde{\gamma}, \quad \frac{\mathrm{d}^3\mathrm{F}}{\mathrm{d}Z^3}(0) = \tilde{\alpha} \quad \text{and} \quad G(0) = \tilde{\beta}. \tag{19}$$

There are three $\mathscr{RE}\mathscr{BC}$ to determine three unknowns $\tilde{\gamma}$, $\tilde{\alpha}$ and $\tilde{\beta}$. In order to solve this consistent system with three given-initial conditions, Eq. (18a), and three assumed initial conditions of Eq. (19) (used in place of Eq. (18b)). We next consider the series solution for the Eq. (17) in the form:

$$\left.\begin{aligned} F\left(Z;\tilde{\gamma},\tilde{\alpha},\tilde{\beta}\right) &= \sum_{n=0}^{\infty} c_n\, Z^n, \\ G\left(Z;\tilde{\gamma},\tilde{\alpha},\tilde{\beta}\right) &= \sum_{n=0}^{\infty} d_n\, Z^n \end{aligned}\right\}. \tag{20}$$

The first few c_i's and d_i's can be obtained from Eqs. (18a) and (19) as:

$$c_0 = 0,\ c_1 = 0,\ c_2 = \tilde{\gamma}/2,\ c_3 = \tilde{\alpha}/6,\ d_0 = 0,\ d_1 = \tilde{\beta}. \tag{21}$$

To obtain the remaining coefficients, we substitute Eq. (20) in Eq. (17) and get the recurrence relations:

$$\left.\begin{aligned} c_{k+4} &= \frac{2a_c^2(k+2)(k+1)c_{k+2} - a_c^4 c_k + a_1^2 a_c^2 Ra_{nl_c}\, d_k}{(k+1)(k+2)(k+3)(k+4)}, \\ d_{k+2} &= \frac{2a_c^2 d_k - \sum_{l=0}^{k} \delta_{l1}\, c_{k-1}}{a_1(k+2)(k+1)} \end{aligned}\right\} \quad k = 0(1)\infty. \tag{22}$$

The above procedure yields:

$$F\left(Z;\tilde{\gamma},\tilde{\alpha},\tilde{\beta}\right) = \frac{\tilde{\gamma}}{2}Z^2 + \frac{\tilde{\alpha}}{6}Z^3 + \left(\frac{2a^2\tilde{\gamma} + a_1^2 a_c^2 Ra_{nl_c}\,\tilde{\beta}}{24}\right)Z^4 + \frac{2a_c^2\tilde{\gamma}}{120}Z^5 + \left(\frac{4a_c^4 + 3a_1^2 a_c^2 Ra_{nl_c}\,\tilde{\beta} - a_c^4\tilde{\gamma}}{720}\right)Z^6 + \ldots \text{ 25 terms}, \tag{23}$$

$$G\left(Z;\tilde{\gamma},\tilde{\alpha},\tilde{\beta}\right) = \tilde{\beta} + \frac{\tilde{\beta}a_c^2}{2}Z^2 + \frac{\left(a_c^4\tilde{\beta}\right)}{24}Z^4 - \frac{1}{20}Z^5 + \frac{\left(-4\tilde{\alpha} + a_c^6\tilde{\beta}\right)}{720}Z^6 + \ldots \text{ 25 terms}. \tag{24}$$

Now, using Eqs. (23) and (24) in the unused $\mathscr{RE}\mathscr{BC}$ condition of Eq. (18b), we get a system of three non-linear algebraic equations in $\tilde{\alpha}$, $\tilde{\beta}$ and $\tilde{\gamma}$ which can be solved by using the three-variable Newton-Raphson method. The convergence of the series solution presented in Eqs. (23) and (24) depends on the number of terms included. It is found that at least 25 terms are necessary to achieve convergence with three-digit-numerical accuracy. Increasing the number of terms beyond 25 terms yields the same three-digit-accurate values of $\tilde{\alpha}$, $\tilde{\beta}$ and $\tilde{\gamma}$. In the next section, we present a procedure to obtain the expression of the eigenfunction for the $X-$independent convective mode.

2.3 Derivation of the eigenfunction, $H(Z)$, for the convective mode

The eigenfunction in this case is $X-$independent thereby meaning it is a function of Z only. The expression of $H(Z)$ can be obtained by solving the following equation:

$$\frac{d^2H}{dZ^2} = \frac{\partial(\Psi,\Theta)}{\partial(X,Z)}. \tag{25}$$

This equation essentially means that the eigenfunction is got by equating the transverse diffusion and convective terms. We mention here that H being a function of Z only, the right-hand-side of Eq. (25) should also be a function of Z only. Keeping this in mind, we now substitute Eq. (16) in Eq. (25). For the right-hand-side of Eq. (25) to be independent of X, we need to have the following enforcement:

$$F'(Z)G(Z) = F(Z)G'(Z). \tag{26}$$

The validity of Eq. (26) for all Z was confirmed through computation. Hence Eq. (25) now yields

$$\frac{d^2H}{dZ^2} = \tilde{\gamma}^2 a_c F'(Z)G(Z). \tag{27}$$

Eq. (27) is next solved for $H(Z)$ subject to:

$$\frac{dH}{dZ}(0) = 0, H(1) = 0. \tag{28}$$

Eq. (28) is, in fact, the $H-$version of the G boundary condition in Eq. (17). The particular solution of Eq. (27) subject to Eq. (28) is

$$H(Z) = \tilde{\gamma}^2 a_c \left[M(Z) + N(0)(1-Z) - M(1)\right], \tag{29}$$

where $M(Z) = \int_Z \left[\int F(\eta)G'(\eta)d\eta\right] dZ$ and $N(Z) = \int_Z F(\eta)G'(\eta)dZ$. We next confirm whether $H(Z)$ is the needed function by checking its orthogonality with $F(Z)$ and $G(Z)$. It can easily be verified that the following orthogonality or otherwise is true:

$$\left.\begin{aligned} \int_0^1 F(\eta)H(\eta)d\eta = 0, \\ \int_0^1 G'(\eta)H(\eta)d\eta = 0, \\ \int_0^1 H^2(\eta)d\eta \neq 0 \end{aligned}\right\}. \tag{30}$$

In the next section, using $H(Z)$ we construct a minimal representation of Fourier-Galerkin series to perform a weakly-nonlinear-stability-analysis of the $\mathscr{I}\mathscr{H}\mathscr{G}$ enabled convection problem and this results in a new-Lorenz-model that structurally resembles the classical one of $\mathscr{R}\mathscr{B}\mathscr{C}$.

2.4 Lorenz model for $\mathscr{I}\mathscr{H}\mathscr{G}$ driven convection

In order to derive the Lorenz model, we consider the minimal Galerkin-Fourier-representation for Ψ and Θ as follows

$$\Psi(X,Z,\tau) = \frac{a_c}{m}\sqrt{\frac{\mathscr{I}_1\mathscr{I}_2}{\mathscr{I}_3\mathscr{I}_4}}\mathscr{A}(\tau)\sin(a_cX)F(Z), \tag{31}$$

$$\Theta(X,Z,\tau) = \frac{a_c\, Ra_{nl}\, Q_2}{mQ_1}\sqrt{\frac{\mathscr{I}_1\mathscr{I}_2}{\mathscr{I}_3\mathscr{I}_4}}\mathscr{B}(\tau)\cos(a_cX)G(Z) - \frac{a_c\, Ra_{nl}\, Q_2\mathscr{I}_1}{m\, Q_1\mathscr{I}_2}\mathscr{C}(\tau)H(Z), \tag{32}$$

where

$$\left.\begin{aligned}
&\mathscr{I}_1 = \int_0^1 FGH'\,dZ, \quad \mathscr{I}_2 = \int_0^1 F'GH\,dZ, \quad \mathscr{I}_3 = \int_0^1 G^2\,dZ, \quad \mathscr{I}_4 = -\int_0^1 H^2\,dZ,\\
&\mathscr{I}_5 = \int_0^1 GG''\,dZ, \quad \mathscr{I}_6 = \int_0^1 HH''\,dZ, \quad m = \frac{\mathscr{I}_5 - a_c^2\mathscr{I}_3}{\mathscr{I}_3},\\
&Q_1 = \frac{\int_0^1 FF''''\,dZ - 2a_c^2\int_0^1 FF''\,dZ + a_c^4\int_0^1 F^2\,dZ}{a_c^2\int_0^1 F^2\,dZ - \int_0^1 FF''''\,dZ},\\
&Q_2 = \frac{a_c\int_0^1 FG\,dZ}{a_c^2\int_0^1 F^2\,dZ - \int_0^1 FF''''\,dZ}
\end{aligned}\right\}, \tag{33}$$

and the eigenfunctions $F(Z)$, $G(Z)$ and $H(Z)$ are given by Eqs. (23), (24) and (29) respectively. Substituting Eqs. (31) and (32) into Eqs. (13) and taking projection of the resulting equations on the three eigenfunctions, we arrive at the scaled Lorenz model for the $\mathscr{I}\mathscr{H}\mathscr{G}$-driven-convection in the form

$$\frac{d\mathscr{A}^*}{d\tau^*} = Pr^*\ [\mathscr{B}^* - \mathscr{A}^*], \tag{34}$$

$$\frac{d\mathscr{B}^*}{d\tau^*} = r\,\mathscr{A}^* - \mathscr{A}^*\mathscr{C}^* - \mathscr{B}^*, \tag{35}$$

$$\frac{d\mathscr{C}^*}{d\tau^*} = -b^*\mathscr{C}^* + \mathscr{A}^*\mathscr{B}^*, \tag{36}$$

where $(\mathscr{A}^*,\mathscr{B}^*,\mathscr{C}^*,\tau^*) = \frac{(\mathscr{A},\mathscr{B},\mathscr{C},\tau)}{m}$, $Pr^* = Pr\,Q_1$, $r = \frac{Ra_{nl}}{Ra_{nlc}}$ and $b^* = \frac{\mathscr{I}_6}{\mathscr{I}_4}$.
Eqs. (34) - (36) exhibit the same properties as that of the classical Lorenz model [25]as it is structurally similar to it.
These properties are

1. In phase-space $(\mathscr{A}^*,\mathscr{B}^*,\mathscr{C}^*)$, the $\mathscr{C}^*$- axis serves as the axis of symmetry since the Lorenz model is invariant under the transformation

$$(\mathscr{A}^*, \mathscr{B}^*, \mathscr{C}^*) \longleftrightarrow (-\mathscr{A}^*, -\mathscr{B}^*, \mathscr{C}^*).$$

2. The system is dissipative in nature since

$$\frac{\partial \dot{\mathscr{A}}^*}{\partial \mathscr{A}^*} + \frac{\partial \dot{\mathscr{B}}^*}{\partial \mathscr{B}^*} + \frac{\partial \dot{\mathscr{C}}^*}{\partial \mathscr{C}^*} = -(Pr^* + 1 + b^*) < 0,$$

where an overdot indicates time derivative.

3. The critical points of the system are given by

$$O = (0,0,0),\ \mathscr{C}^+ = \left(\sqrt{(r-1)b^*}, \sqrt{(r-1)b^*}, r-1\right),$$
$$\mathscr{C}^- = \left(-\sqrt{(r-1)b^*}, -\sqrt{(r-1)b^*}, r-1\right)$$

To determine the onset of chaos, we have to find the Hopf Rayleigh number, r_H. On comparing our scaled generalised Lorenz model for the $\mathscr{IHG}$ driven convection with the classical one[25], we can write the expression for r_H as

$$r_H = Pr^*\left(\frac{Pr^* + b^* + 3}{Pr^* - b^* - 1}\right). \tag{37}$$

We next derive the Stuart–Landau equation from Eqs. (34)-(36). From Eqs.(35) and (36), $\mathscr{B}^*$ and $\mathscr{C}^*$ can be obtained in terms of $\mathscr{A}^*$ as follows:

$$\mathscr{B}^*(\tau^*) = \mathscr{A}^* + \frac{1}{Pr^*}\frac{d\mathscr{A}^*}{d\tau^*}, \tag{38}$$

$$\mathscr{C}^*(\tau^*) = \frac{1}{\mathscr{A}^*}\left[(r-1)\mathscr{A}^* - \left(\frac{1}{Pr^*} + 1\right)\frac{d\mathscr{A}^*}{d\tau^*} - \frac{1}{Pr^*}\frac{d^2\mathscr{A}^*}{d\tau^{*2}}\right]. \tag{39}$$

Substituting Eqs.(38) and (39) in Eq.(36) and neglecting $\frac{d^3\mathscr{A}^*}{d\tau^{*3}}$, $\frac{d^2\mathscr{A}^*}{d\tau^{*2}}\frac{d\mathscr{A}^*}{d\tau^*}$, and $\mathscr{A}^*\frac{d^2\mathscr{A}^*}{d\tau^{*2}}$, we get the Stuart–Landau equation in the form

$$\frac{d\mathscr{A}^*}{d\tau^*} = \frac{Pr^*}{b^*(1+Pr^*)}\left[(r-1)b^* - \mathscr{A}^{*2}\right]\mathscr{A}^*. \tag{40}$$

Equation (40) is a Bernoulli equation in $\mathscr{A}$ and it can be solved using $\mathscr{A}(0) = 1$, and its particular solution is then given by

$$\mathscr{A}^*(\tau^*) = \left[\frac{1}{(r-1)b^*} + \left(1 - \frac{1}{(r-1)b^*}\right)e^{-\frac{2(r-1)}{1+\mathrm{Pr}^*}\tau^*}\right]^{-\frac{1}{2}}. \tag{41}$$

2.5 Estimate of the Nusselt Number

To estimate the heat-transport, we use the thermal- Nusselt-number, Nu_{nl},definition:

$$Nu_{nl}(\tau^*) = \left[\frac{\int_0^{2\pi} \left(k_{bl} \frac{dT_b}{dZ} + k_{nl} \frac{\partial \Theta}{\partial Z} \right) dX}{k_{bl} \int_0^{2\pi} \frac{dT_b}{dZ} dX} \right]_{Z=0}. \tag{42}$$

Substituting the non-dimensional form of Eq.(9) and Eq.(23) in Eq.(42) and completing the integration, we get

$$Nu_{nl}(\tau^*) = 1 + \frac{k_{nl}}{k_{bl}} H''(0) \mathscr{C}^*(\tau^*), \tag{43}$$

where $\mathscr{C}^*(\tau^*)$ in terms of $\mathscr{A}^*(\tau^*)$ is given by Eq.(39). We now proceed to discuss the results.

3 Results and discussion

This work examines both linear and nonlinear aspects of stability in nanoliquid convection effected by $\mathscr{IHG}$. Palm oil based nanofluids with Cu or TiO_2 are analyzed using thermophysical properties based on mixture theory and phenomenological relations. The effects of nanoparticle concentration, nanoparticle type, and key properties such as thermal conductivity, specific heat, and thermal expansion are studied to understand their role on the onset of regular convection, heat transfer and chaotic motion. The findings are compared using variations in the Nusselt and modified Rayleigh numbers for two nanoliquid combinations. In the current study we have used Palm oil as a baseliquid. Palm oil serves as an effective and sustainable base liquid for nanoliquid applications due to its favorable thermophysical and environmental characteristics. As a naturally derived and biodegradable fluid, palm oil gives us an eco-friendly option compared to synthetic or mineral oils. It has a good thermal stability and high viscosity which makes it suitable for use at higher temperatures while maintaining reliability. One of the real advantages of palm oil is its versatility, it can pair effectively with a wide range of nanoparticles to form stable nanoliquids that significantly boost thermal conductivity. Added to that is its low cost and wide spread availability, and sustainable option for heat transfer applications.

In this study, the nanoliquid Rayleigh number is determined using effective thermophysical properties based on mixture theory, phenomenological models, and experimental data from previous works. Tables 1 and 2 list the properties of the Palm-oil and the two nanoparticles, Cu and TiO_2, and these documented values used to calculate the modified Rayleigh number, and thermophysical properties of the two nanoliquids under consideration are documented in Table 3. Next using the relations (4)–(5), a dimensionless factor F was introduced to rearrange the expression of the Rayleigh number to ascertain the influence of nanoparticle concentration and fluid characteristics on onset of regular convection. The factor $F = \frac{(1-\alpha)^{2.5}(\rho\beta)_{nl}}{a_1 \rho_{bl} \beta_{bl}}$ governs the critical threshold for the onset of regular (pre-chaotic) convection. Values of F, for Palm-oil-Cu and Palm-oil-TiO_2 nanoliquids at different volume fractions are given in Table 4. The factor F helps in understanding the advanced onset of pre-chaotic-motion due to the presence

of nanoparticles. Values of F determine whether onset is advanced or delayed. At a nanoparticle concentration of 0.02, the Palm-oil-Cu nanoliquid exhibits a slightly higher F value (0.9011) compared to that of Palm-oil-TiO_2 (0.8978), suggesting an earlier onset of convection in the case of Palm-oil-Cu. With an increase in concentration to 0.03 and 0.04, both nanoliquids show a steady decrease in F. For Palm-oil-Cu, F decreases from 0.9011 to 0.8115, while for Palm-oil-TiO_2, it drops from 0.8978 to 0.8056. This reduction is mainly because of the rise in viscosity and increased particle interactions for higher concentration of nanoparticles which leads to the suppression of fluid motion. The results suggest that the thermal conductivity and the viscosity influence convection in an opposing fashion. When a small fraction of nanoparticles is added, the liquid's ability to transfer heat improves noticeably. To achieve efficient heat transport, it is important to choose nanoparticle–base fluid combinations that yield relatively high F values.

Figure 2 shows the variation of the normalized Nusselt number (Nu_{nl}) with the time (τ^*) in the case of pre-chaotic motion for Palm-oil-Cu nanoliquid at different nanoparticle volume fractions $(\alpha = 0.02, 0.03, \text{ and } 0.04)$. Figure 3 shows the variation of the Nusselt number (Nu_{nl}) with the time (τ^*) for Palm-oil-TiO_2 nanoliquid at different nanoparticle volume fractions $(\alpha = 0.02, 0.03, \text{ and } 0.04)$. The results reveal that the heat transfer slightly increases with increasing nanoparticle concentration. This enhancement is attributed to the improved effective thermal conductivity and thermal diffusivity of the nanoliquid at higher volume fractions.

Values of r_H for volume fraction, $\alpha = 0.04$ are given in Table 5. These values are very high for nanoliquids since the Pr values are very large and hence we can come to the conclusion that onset of chaotic convection is delayed in the case of Palm-Oil-based nanoliquids. This characteristic of nanoliquids is very useful to maintain the stability of the system.

Table 1: Values of thermophysical properties of Palm-oil at room temperature (300K).

Quantity	Palm-oil
Density (ρ_{bl}) [kg/m^3]	885[26]
Thermal expansion coefficient (β_{bl}) [$K^{-1} \times 10^5$]	7.27*
Specific heat ($C_{p_{bl}}$) [J/kgK]	1875[26]
Thermal-conductivity (k_{bl}) [W/mK]	8.4[26]
Dynamic-viscosity (μ_{bl}) [kg/m-s]	0.485[26]

* Estimated value from available related data

4 Conclusion

The conclusions of the study are presented as follows:

1. Industry and kitchen wastes can be utilised in automobiles as thermal coolants.

Table 2: Values of thermophysical properties of Copper and Titanium dioxide nanoparticles at room temperature (300K).

Quantity	Copper[27]	Titanium dioxide[27], [28]
Density (ρ_{np}) [kg/m^3]	8933.00	4157.00
Thermal expansion coefficient $(\beta_{np})[K^{-1} \times 10^5]$	0001.67	0002.87
Specific heat $(C_{p_{np}})$ [J/kgK]	0385.00	0710.00
Thermal-conductivity (k_{np})[W/mK]	0401.00	0008.40

Table 3: Thermophysical properties of Palm-oil-based nanoliquids for different volume fractions.

Nanoliquids	α	ρ_{nl}	k_{nl}	μ_{nl}	$(C_p)_{nl}$	$\beta_{nl} \times 10^{-5}$	$\alpha_{nl} \times 10^7$	Pr_{nl}
Palm-oil–Cu	0.02	1045.96	0.152807	0.510125	1620.49	60.5674	0.90153	5409.81
Palm-oil–TiO_2		0950.80	0.152369	0.510125	1772.69	66.5673	0.90402	5934.87
Palm-oil–Cu	0.03	1126.44	0.157346	0.523374	1520.52	55.8013	0.91866	5057.64
Palm-oil–TiO_2		0983.70	0.156677	0.523374	1726.67	63.8086	0.92243	5767.87
Palm-oil–Cu	0.04	1206.92	0.161980	0.537111	1433.87	51.6709	0.93599	4754.59
Palm-oil–TiO_2		1016.60	0.161070	0.537111	1683.62	61.2285	0.94106	5604.43

Table 4: Values of the factor, F.

Nanoliquids	$\alpha = 0.02$	$\alpha = 0.03$	$\alpha = 0.04$
Palm-oil–Cu	0.901114	0.855196	0.811467
Palm-oil–TiO_2	0.897799	0.850506	0.805570

Table 5: Values of r_H for nanoliquids with $\alpha = 0.04$.

Nanoliquids	Pr_{nl}	b^*	r_H
Palm-oil–Cu	4754.59	0.112798	242578
Palm-oil–TiO_2	5604.43	0.118502	222797

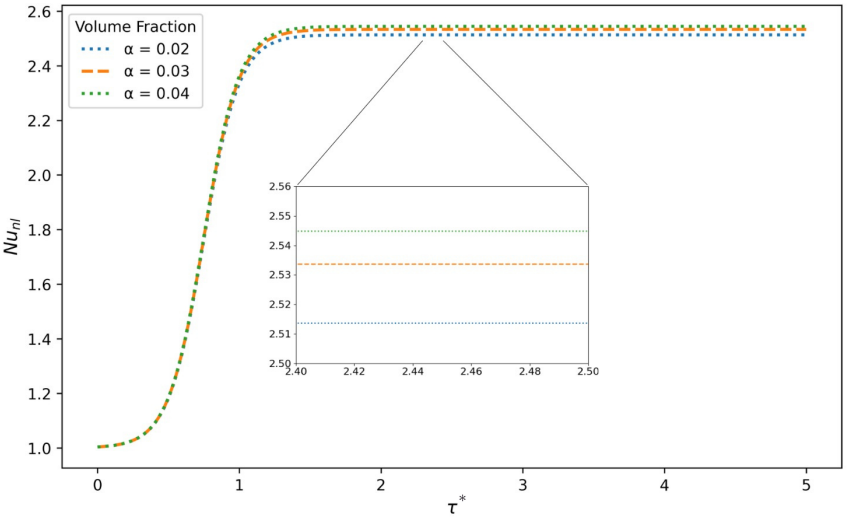

Figure 2: Plot of Nu_{nl} versus τ^* for $Palm-oil-Cu$ nanoliquid for different volume fractions.

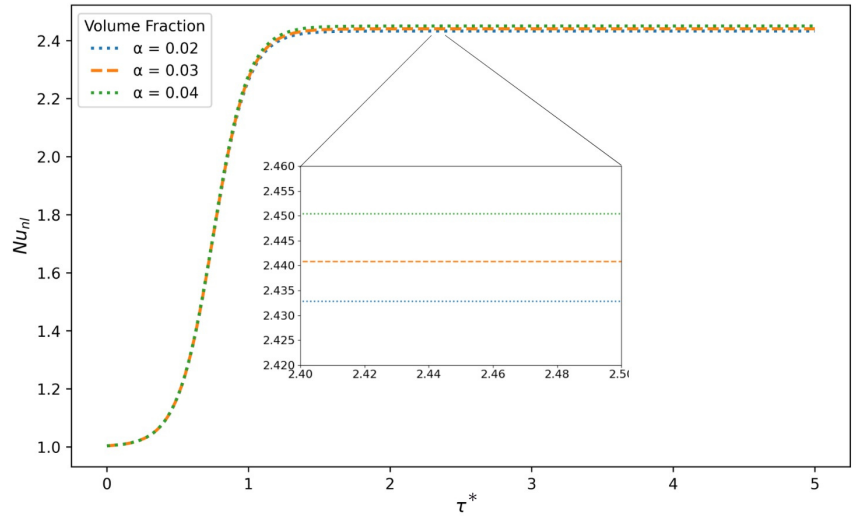

Figure 3: Plot of Nu_{nl} versus τ^* for $Palm-oil-TiO_2$ nanoliquid for different volume fractions.

2. Palmoil-based nanoliquids have very high viscosity and are hence stable in application situations.

References

[1] Tritton D. J. and Zarraga M. N., "Convection in horizontal layers with internal heat generation. Experiments", *Journal of Fluid Mechanics*, vol. 30, (1), pp. 21–31, 1967.

[2] Roberts P. H., "Convection in horizontal layers with internal heat generation. Theory", *Journal of Fluid Mechanics*, vol. 30, (1), pp. 33–49, 1967.

[3] Thirlby R, "Convection in an internally heated layer", *Journal of Fluid Mechanics*, vol. 44, (4), pp. 673–693, 1970.

[4] Schwiderski E. W., "Bifurcation of convection in internally heated fluid layers", *Physics of Fluids*, vol. 15, (11), pp. 1882–1898, 1972.

[5] Peckover R. S. and Hutchinson I. H., "Convective rolls driven by internal heat sources", *Physics of Fluids*, vol. 17, (7), pp. 1369–1371, 1974.

[6] Gasser R. and Kazimi M., "Onset of convection in a porous medium with internal heat generation", *Journal of Heat Transfer*, vol. 98, (1), pp. 49–54, 1976.

[7] Hamabata H. and Takashima M., "The effect of rotation on convective instability in a horizontal fluid layer with internal heat generation", *Journal of the Physical Society of Japan*, vol. 52, (12), pp. 4145–4151, 1983.

[8] Tasaka Y. and Takeda Y., "Effects of heat source distribution on natural convection induced by internal heating", *International Journal of Heat and Mass Transfer*, vol. 48, (6), pp. 1164–1174, 2005.

[9] Kuznetsov A. and Nield D., "The effect of spatially nonuniform internal heating on the onset of convection in a horizontal fluid layer", *Journal of Heat Transfer*, vol. 138, (6), p. 062 503, 2016.

[10] Goluskin D. and Poel E. P. Van der, "Penetrative internally heated convection in two and three dimensions", *Journal of Fluid Mechanics*, vol. 791, p. R6, 2016.

[11] Wang Q., Lohse D., and Shishkina O., "Scaling in internally heated convection: A unifying theory", *Geophysical Research Letters*, vol. 48, (4), p. e2020GL091198, 2021.

[12] Deepika N., Narayana P. A. L., and Hill A. A., "Onset of Darcy-Brinkman convection with a uniform internal heat source and vertical throughflow", *International Journal of Thermal Sciences*, vol. 117, pp. 136–144, 2017.

[13] Choi S. and Eastman J., "Enhancing thermal conductivity of fluids with nanoparticles", *Proceedings of the ASME International Mechanical Engineering Congress and Exposition*, vol. 66, Jan. 1995.

[14] Eastman J. A., Choi S., Li S., Yu W, and Thompson L. J., "Anomalously increased effective thermal conductivities of ethylene glycol-based nanofluids containing copper nanoparticles", *Applied Physics Letters*, vol. 78, (6), pp. 718–720, 2001.

[15] Das S. K., Putra N. S. D., Thiesen P., and Roetzel W., "Temperature dependence of thermal conductivity enhancement for nanofluids", *Journal of Heat Transfer*, vol. 125, (4), pp. 567–574, 2003.

[16] Buongiorno J., "Convective transport in nanofluids", *Journal of Heat Transfer*, vol. 128, (3), pp. 240–250, Aug. 2005.

[17] Khanafer K., Vafai K., and Lightstone M., "Buoyancy-driven heat transfer enhancement in a two-dimensional enclosure utilizing nanofluids", *International Journal of Heat and Mass Transfer*, vol. 46, (19), pp. 3639–3653, 2003.

[18] Siddheshwar P. G. and Meenakshi N, "Amplitude equation and heat transport for Rayleigh–Bénard convection in Newtonian liquids with nanoparticles", *International Journal of Applied and Computational Mathematics*, vol. 3, (1), pp. 271–292, 2017.

[19] Siddheshwar P. G., Kanchana C, Kakimoto Y, and Nakayama A., "Steady finite-amplitude Rayleigh–Bénard convection in nanoliquids using a two-phase model: Theoretical answer to the phenomenon of enhanced heat transfer", *Journal of Heat Transfer*, vol. 139, (1), p. 012 402, 2017.

[20] Kanchana C and Laroze D., "Study of chaos in rayleigh-benard convection of water-alumina nanofluid with heat source sink", *CU Journal of Non-Linear Fluid Mechanics*, vol. 1, (01), pp. 1–15, 2025.

[21] Siddheshwar P. G., Narayana M., Laroze D., and Kanchana C, "Brinkman–bénard convection with rough boundaries and third-type thermal boundary conditions", *Symmetry*, vol. 15, (8), p. 1506, 2023.

[22] Siddheshwar P. G., Kanchana C., Pérez L. M., and Laroze D., "Influence of symmetric/asymmetric boundaries on axisymmetric convection in a cylindrical enclosure in the presence of a weak vertical throughflow", *Communications in Nonlinear Science and Numerical Simulation*, vol. 126, p. 107 495, 2023.

[23] Firdose H., Siddheshwar P. G., and Idris R., "Effects of rough boundaries on Rayleigh–Bénard convection in nanofluids", *ASME Journal of Heat and Mass Transfer*, vol. 145, (6), p. 062 602, 2023.

[24] Kruthik P. S., Idris R., and Siddheshwar P. G., "Study of the linear and nonlinear regimes of natural convection with weak or dominating internal heat generation for rigid-free boundaries", *Journal of Porous Media*, vol. 28, (9), pp. 21–39, 2025.

[25] Lorenz E. N., "Deterministic nonperiodic flow", *Journal of Atmospheric Sciences*, vol. 20, (2), pp. 130 –141, 1963.

[26] Hussein A. M., Lingenthiran, Kadirgamma K, Noor M., and Aik L., "Palm oil based nanofluids for enhancing heat transfer and rheological properties", *Heat and Mass Transfer*, vol. 54, (10), pp. 3163–3169, 2018.

[27] Bergman T. L., *Fundamentals of Heat and Mass Transfer*. New York, NY: John Wiley & Sons, 2011.

[28] Hummer D. R., Heaney P. J., and Post J. E., “Thermal expansion of anatase and rutile between 300 and 575 k using synchrotron powder x-ray diffraction”, *Powder Diffraction*, vol. 22, (4), pp. 352–357, 2007.

Acknowledgements

Author is thankful to Christ University for their support.

Data Availability

The authors declare that no data was generated.